Stereoscopic-Based Mass Properties Estimation for Warhead Fragments

Alessia Nocerino

Katharine Larsen

Riccardo Bevilacqua

Elisabetta L. Jerome

AIAA JOURNAL
Vol. , No. ,

Technical Notes

Stereoscopic-Based Mass Properties Estimation for Warhead Fragments

Alessia Nocerino[*]
University of Naples "Federico II," 80056 Naples, Italy
Katharine E. Larsen[†] and Riccardo Bevilacqua[‡]
Embry-Riddle Aeronautical University, Daytona Beach, Florida 32114
and
Elisabetta L. Jerome[§]
Air Force Test Center, Eglin Air Force Base, Florida 32542

https://doi.org/10.2514/1.J062703

I. Introduction

FRAGMENTATION characteristics such as spatial distribution, number of fragments, fragment velocity, and fragment mass can be used to characterize the lethality of a fragmenting weapon or any metal cased explosive [1,2]. However, most warhead tests and evaluations are limited to static arena testing, where fragment characteristics must be collected by hand. Recently, stereoscopic imaging techniques have been added to static arena tests. Using this method, position tracks can be collected for each fragment, and then velocity information can be found. This paper proposes a method to estimate the mass and moment of inertia using data collected by a stereoscopic imaging system. Tracking the fragments using this system can increase the number of fragments collected and reduce the need for manual fragment collection.

Static arena testing is based on standard test operating procedures consisting of a warhead placed at the center of a testing arena surrounded by fragment collection media, and collection of fragmentation characteristics. Previously, static arena tests included fragment witness panels, such as Celotex bundles, which may include measurement equipment, such as pressure gauges [3]. Then, fragment shape, size, mass, and location rely on on-the-field manual collection. Arena tests are high in labor and financial costs.

Recently, stereoscopic imaging has become an addition to the classic static arena test. High-speed stereoscopic imaging utilizes multiple different camera angles to provide two-dimensional images with depth, essentially giving the image three-dimensional qualities [4]. One stereoscopic imaging system, known as the Optical Warhead Lethality Sensor Suite (OWLSS), has been developed by Torch Technologies. OWLSS tracks the position vectors of individual fragments from which the velocity vectors can be calculated [5]. Despite its potential, this new methodology will not be complete until it can also estimate the fragment mass properties within a certain tolerance. The core motivation for this study is to be able to calculate the mass properties of the fragments from stereoscopic data, thus eliminating the need for the time consuming and expensive fragment hand collection.

In addition to physical fragmentation tests, simulations can be used to predict fragmentation characteristics as well. One fragmentation computer program is known as CALE. It predicts numerical models for fragment mass and velocity distribution [6,7]. Following CALE, Picatinny Arsenal developed Picatinny Arsenal Fragmentation (PAFRAG). Using CALE and PAFRAG, Picatinny Arsenal estimates lethality and a safe separation distance [2,8]. The United States Naval Air Warfare Center's Weapons Division (NAWCWD) has also developed a simulation model, which given experimental data can produce trajectories for dynamic weapon fragmentation. While these simulation methods can provide the user with general weapon information, they require some data for initialization, from either experimentation, such as static arena testing, or fragmentation formulas.

One of the fragmentation formulas used to inform these simulation methods is Mott's equation. Mott presented a formula to predict the number of fragments produced from a naturally fragmenting metal shell casing of a weapon. This formula is highly dependent on casing material [9]. The following equation is one version of Mott's two-dimensional fragmentation distribution law:

$$N(m) = N_0 \exp\left[-\frac{(m)^{\frac{1}{2}}}{M_A}\right] \tag{1}$$

where N is the number of fragments with mass greater than m and N_0 is the total number of fragments created, calculated using

$$N_0 = \frac{M}{2M_A^2} \tag{2}$$

where M is the casing mass and M_A is the casing size parameter. For a thin casing, the size parameter can be found using casing measurements as

$$M_A = B_m t^{\frac{5}{6}} d^{\frac{1}{3}}\left(1 + \frac{t}{d}\right) \tag{3}$$

where B_m is the material constant, t is the thickness of the casing, and d is the outer diameter of the casing [10]. Knowing the total casing mass, one could calculate the average fragment mass. However, this is under the assumption that Mott's formula predicts the correct number of fragments, and while it can predict the general distribution of fragments, smaller fragments are often excluded.

Following Mott's total number of fragments formula, similar formulas were presented to estimate the cumulative fragment masses with more accuracy. One paper, published in 2009, compares some of these distribution formulas: Mott, generalized Mott, Grady, generalized Grady, Lognormal, Weibull, and Held distributions [11]. They found that the generalized Grady distribution provided the best mass estimation for their dataset. However, the accuracy of these formulas may be dependent on the casing material. Again, these estimations are for the cumulative mass of all the fragments, and while the average mass can be calculated, one cannot calculate the exact mass of each fragment.

This paper presents a strategy for the mass and moment of inertia estimation of fragments deriving from a warhead's detonation event. The presented procedure exploits estimated motion and presented

Received 5 December 2022; revision received 24 April 2023; accepted for publication 12 June 2023; published online XX epubMonth XXXX.

*Ph.D. Candidate, Department of Industrial Engineering.
†Ph.D. Candidate, Aerospace Engineering Department, 1 Aerospace Boulevard.
‡Professor, Aerospace Engineering Department, 1 Aerospace Boulevard; bevilacr@erau.edu. Associate Fellow AIAA (Corresponding Author).
§Technical Advisor for Armament and Weapons Test and Evaluation, 101 West D Avenue, Building 1, Suite 115.

area data obtained by processing images acquired by a stereoscopic vision system tracking the fragments. Specifically, the mass estimation procedure relies on the second dynamics principle applied at multiple observation instants, while the moments of inertia are determined by solving with a least square approach, a linear system based on the expression of the angular momentum vector in the inertial frame. Performance assessment of the presented strategies is then carried out in a numerical simulation environment in which all the relevant perturbations and uncertainties can be included. Additionally, the accuracy of the mass estimation strategies can also be verified by exploiting two sets of experimental data. With these estimates, warhead evaluation methods, both experimental and simulated, can be improved. The following section, Sec. II, describes the proposed approach. Sections III and IV present the simulation, numerical, and experimental validation results. Finally, Sec. V presents the conclusions.

II. Estimate of the Mass Properties of a Fragment

By processing raw data collected by a multiple stereovision system (e.g., a suite of electro-optical sensors) for a fragment deriving from an explosive event, it is possible to obtain information about the fragment's motion (i.e., position, velocity, attitude, and angular velocity) and presented area. Then, it is possible to obtain an estimate of both mass and inertia of the observed fragment.

A. Mass Estimate

It is reasonable to assume that a high-velocity fragment moving at an altitude above ground of a few meters is subject only to the gravitational and drag forces. Thus, according to the Newton's law, the following equation is valid in an inertial frame:

$$\boldsymbol{F}(t_k) = m\boldsymbol{a}(t_k) = m\boldsymbol{g} - \frac{1}{2}\rho V(t_k)^2 S(t_k) C_d \hat{\boldsymbol{v}}(t_k) \tag{4}$$

where
- $\boldsymbol{F}(t_k)$ is the resulting force acting on the fragment at time instant t_k;
- m is the fragment's mass;
- $\boldsymbol{a}(t_k)$ is the instantaneous acceleration of the fragment;
- $\boldsymbol{g}$ is the gravity acceleration vector;
- P is the air density;
- $V(t_k)$ is the instantaneous norm of the velocity vector and $\hat{\boldsymbol{v}}(t_k)$ its direction in the considered inertial frame;
- $S(t_k)$ is the cross-sectional area of the fragment; and
- C_d is the drag coefficient.

It is worth noting that the cross-sectional area is a time-varying parameter, as the fragment rotates at a nonnegligible angular velocity.

Equation (4) can be projected along one of the inertial axes and the acceleration can be approximated by a first order numerical derivative of the estimated velocity, obtaining the following equation:

$$\begin{aligned} F_z(t_k) &= ma_z(t_k) = m\frac{v_{z,k} - v_{z,k-1}}{t_k - t_{k-1}} \\ &= mg_z - \frac{1}{2}\rho V(t_k)^2 S(t_k) C_d \hat{\boldsymbol{v}}_z(t_k) \end{aligned} \tag{5}$$

If all the required parameters were known with no uncertainty or noise, the mass could be estimated by modifying Eq. (5) as follows:

$$m = \left| \frac{\frac{1}{2}\rho V(t_k)^2 S(t_k) C_d \hat{\boldsymbol{v}}_z(t_k)}{a_z(t_k) - g} \right| \tag{6}$$

However, the velocity, acceleration data, and shape are estimated by processing the vision-based data and thus are affected by noise, while for the drag coefficient modeled on the basis of reference [12], an estimate of the mass of the fragment can instead be obtained as the mean value of different observations, as in Eq. (7).

$$m = \frac{1}{N}\sum_{k=1}^{N} \left| \frac{\frac{1}{2}\rho V(t_k)^2 S(t_k) C_d \hat{\boldsymbol{v}}_z a_z(t_k)}{a_z(t_k) - g} \right| \tag{7}$$

where N is the number of the observations considered.

B. Inertia Estimate

A similar approach can be applied to estimate the moments of inertia. As for the inertia estimate of space debris, the expression of the angular momentum in the inertial frame can be exploited [13–16]. The main difference is that, in this case, it is not possible to apply the freely tumbling rigid body assumption. The angular momentum vector in the inertial frame is given by

$$\underline{\underline{R}}^{\mathrm{IRF}}_{\mathrm{BRF}} \underline{\underline{I}}\boldsymbol{\omega} = \begin{bmatrix} R_{11} & R_{12} & R_{13} \\ R_{21} & R_{22} & R_{23} \\ R_{31} & R_{32} & R_{33} \end{bmatrix} \begin{bmatrix} I_{xx} & I_{xy} & I_{xz} \\ I_{xy} & I_{yy} & I_{yz} \\ I_{xz} & I_{yz} & I_{zz} \end{bmatrix} \begin{bmatrix} \omega_x \\ \omega_y \\ \omega_z \end{bmatrix} = \begin{bmatrix} h_x^{\mathrm{IRF}} \\ h_y^{\mathrm{IRF}} \\ h_z^{\mathrm{IRF}} \end{bmatrix} \tag{8}$$

where $\underline{\underline{R}}^{\mathrm{IRF}}_{\mathrm{BRF}}$ is the direction cosine matrix describing the orientation of a fragment-fixed reference frame (BRF) with respect to an inertial frame (IRF), $\underline{\underline{I}}$ is the moment of inertia matrix, and $\boldsymbol{\omega}$ the inertial angular velocity of the fragment expressed in BRF. Reorganizing the system in Eq. (8), one can get

$$\begin{bmatrix} R_{11}\omega_x & R_{11}\omega_y + R_{12}\omega_x & R_{11}\omega_z + R_{13}\omega_x & R_{12}\omega_y & R_{12}\omega_z + R_{13}\omega_y & R_{13}\omega_z \\ R_{21}\omega_x & R_{21}\omega_y + R_{22}\omega_x & R_{21}\omega_z + R_{23}\omega_x & R_{22}\omega_y & R_{22}\omega_z + R_{23}\omega_y & R_{23}\omega_z \\ R_{31}\omega_x & R_{31}\omega_y + R_{32}\omega_x & R_{31}\omega_z + R_{33}\omega_x & R_{32}\omega_y & R_{32}\omega_z + R_{33}\omega_y & R_{33}\omega_z \end{bmatrix} \begin{bmatrix} I_{xx} \\ I_{xy} \\ I_{xz} \\ I_{yy} \\ I_{yz} \\ I_{zz} \end{bmatrix} = \begin{bmatrix} h_x^{\mathrm{IRF}} \\ h_y^{\mathrm{IRF}} \\ h_z^{\mathrm{IRF}} \end{bmatrix} \tag{9}$$

which represents a linear system in the form $\underline{\underline{A}}\boldsymbol{x} = \boldsymbol{b}$, which can be solved to estimate the fragment's moments of inertia. While the attitude and angular velocity measurements can be obtained directly from processing stereo images, some considerations must be made for the angular momentum vector term. Indeed, it is not straightforward to get an estimate of the instantaneous angular momentum vector; however, it is possible to consider the system in Eq. (9) in any two different time instants t_1 and t_2:

$$\begin{cases} \underline{\underline{A}}(t_1)\boldsymbol{x} = \boldsymbol{b}(t_1) \\ \underline{\underline{A}}(t_2)\boldsymbol{x} = \boldsymbol{b}(t_2) \end{cases} \tag{10}$$

Then, these two systems can be linearly combined to obtain

$$\Delta\underline{\underline{A}}\boldsymbol{x} = \Delta\boldsymbol{b} \tag{11}$$

where the term $\Delta\boldsymbol{b}$ can be computed as in Eq. (12),

$$\Delta \boldsymbol{b} = \int_{t_1}^{t_2} \boldsymbol{M}(t)\mathrm{d}t \tag{12}$$

and $\boldsymbol{M}(t)$ is the instantaneous torque acting on the target.

In the scenarios under study, it can be assumed that the only torque acting on the fragment is the aerodynamic torque. Its rough estimate can be obtained as the sum of the torque acting on the infinitesimal element volume as follows [17]:

$$T = \sum_{i=1}^{V} 0.5\rho C_d S V^2 (\hat{\boldsymbol{v}} \times (\boldsymbol{O}_i - \boldsymbol{CM})) \tag{13}$$

where V is the number of elements discretizing the volume, $\boldsymbol{O}_i$ center of the ith element volume, and $\boldsymbol{CM}$ is the center of mass of the fragment.

It is important to underline that the system in Eq. (11) can be solved provided that the rank of the matrix $\Delta\underline{\underline{A}}$ is at least equal to the number of the unknowns, i.e., 6. Thus, four different observations are required to estimate the moments of inertia of the fragment. In this work, a least square solver is used to solve the system in Eq. (11), and more than the minimum required observations are considered to reduce the influence of the noise and parameters uncertainty on the final results.

III. Simulation Environment, Scenario, and Numerical Results

A. Simulation Environment and Scenario

This section aims to describe the numerical simulation environment built to generate the synthetic data. Indeed, being the description and evaluation of the extraction of fragment's data from stereo images, its trajectory has been simulated in a numerical simulation environment to which different level of uncertainties will be added. These data are used to test the moments of inertia and mass estimate approaches presented in Sec. II. A schematic representation of the simulation environment is depicted in Fig. 1. The inputs are the fragment's presented area and mass properties. Those, along with the velocity and attitude, are used to model both the aerodynamic force and torque according to the model reported in Eqs. (4) and (13), respectively. While the 3-degree-of-freedom (3-DOF) translational motion of the fragment is modeled through Eq. (4), the rotational dynamics is modeled using a set of translational dynamic equations in the BRF coordinate:

$$\dot{\boldsymbol{\omega}} = \underline{\underline{I}}(M - \boldsymbol{\omega} \times \underline{\underline{I}}\boldsymbol{\omega}) \tag{14}$$

Table 1 Initial condition for the synthetic data generation of the fragment

State parameter	Initial condition
Position, m	$p_0 = [0 \quad 0 \quad 0]$
Velocity, $\mathrm{m} \cdot \mathrm{s}^{-1}$	$v_0 = [-59.56 \quad 814.35 \quad 433.53]$
Attitude, °	$\underline{\underline{R}}_{\mathrm{IRF}}^{\mathrm{BRF}} = \begin{bmatrix} 1 & 0 & 0 \\ 0 & 1 & 0 \\ 0 & 0 & 1 \end{bmatrix}$
Angular velocity, $^\circ \cdot \mathrm{s}^{-1}$	$\omega_0 = [4000 \quad 5000 \quad 3500]$

$$\dot{\boldsymbol{q}} = \frac{1}{2}[0 \quad \boldsymbol{\omega}] \otimes \boldsymbol{q} \tag{15}$$

where $\boldsymbol{q}$ is the attitude quaternion describing the orientation of BRF with respect to the inertial frame.

Starting from the initial condition listed in Table 1, both rotational and translational motion of a cuboid-shaped fragment of 10 cm length is propagated for 0.024 s, assuming that a total of 160 observations are obtained from a multiple stereo-vision systems within the simulation time. Both the velocity and angular velocity initial values have been set considering realistic values for the scenario under study. The drag coefficient of the fragments has been assumed constant over the whole simulation time and equal to 2: this assumption has only been considered for the generation of a reference trajectory of the fragment in order to assess the performance of the proposed approach. The effect of a time-varying drag coefficient is then evaluated by considering experimental data, where, clearly, the real C_d of the fragment comes into play.

Given the limited time of observation, the sensor-fixed reference frame can be considered as an inertial frame. The mass of the fragment is 1.3 kg and its inertia matrix (assuming a nonuniform distribution of the mass) is

$$\underline{\underline{I}} = \begin{bmatrix} 8 & 0 & 0 \\ 0 & 2.5 & 0 \\ 0 & 0 & 5 \end{bmatrix} \mathrm{kg} \cdot \mathrm{m}^2 \tag{16}$$

B. Mass Estimate: Simulation Results

To verify the performance of the mass estimation procedure, a sensitivity analysis on how accuracy in the estimate of the fragment's parameters from stereo images (i.e., area and velocity) and its drag coefficient affect the mass estimate is presented in this section. Specifically, by looking at Eq. (4), it can be noted that the uncertainty

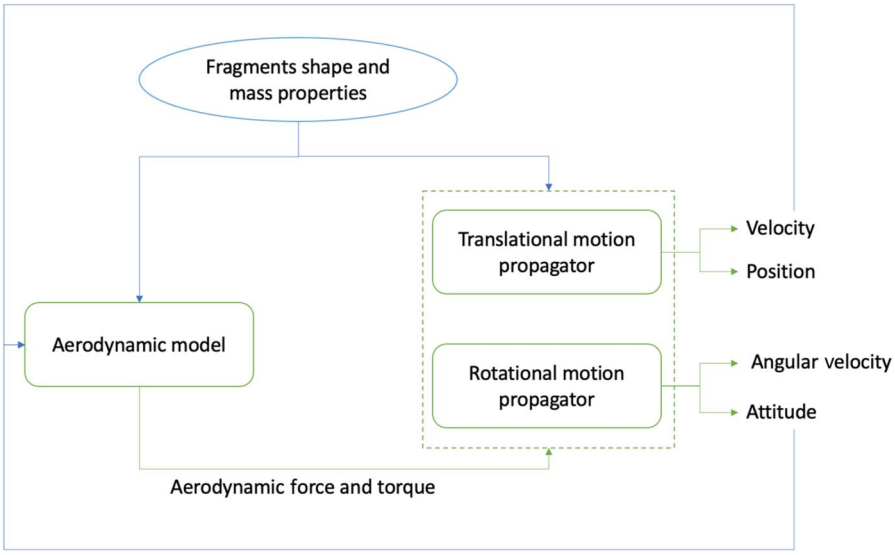

Fig. 1 Block scheme of the numerical simulation environment for synthetic data generation.

on the drag coefficient and fragment's area influence equally the accuracy in the estimate on the drag force acting on the fragment. This is the reason why in the following simulation an uncertainty on the product between the drag coefficient and fragment's area, SC_d, is considered. Specifically, a Gaussian white noise with standard deviation equal to 10, 20, 30, and 40% of the real value. Moreover, since in a realistic application those data will be processed off-line it is assumed that the atmospheric density is a known value. Additionally, a gaussian white noise with standard deviation equal to 10 m/s has been considered to simulate the performance of the velocity estimation from stereo-images. The effect of these uncertainties has been combined to assess the performance of the proposed approach. For the sake of clarity, the uncertainties considered for the sensitivity analysis are reported in Table 2. It is worth underlining that, for the purpose mass estimation, Eq. (7) is projected along a direction perpendicular to the image plane of the stereovision system; thus the area of the fragments projected on the image plane and the component of the velocity perpendicular to it are considered.

Table 2 Standard deviation of the simulated uncertainty on the fragment's velocity and SC_d (the percentage values in the standard deviation column are referred to as the reference value)

Parameter	Standard deviation
SC_d, m^2	10%, 20 %, 30%, 40%
Velocity, $m \cdot s^{-1}$	10

Table 3 Statistics for the mass estimation errors corresponding to different levels of uncertainty in SC_d (statistics are evaluated over 1000 simulations)

Standard deviation		Mean of percentage errors, %	Standard deviation of percentage errors, %
Velocity, m/s	SC_d, %		
10	10	8	6
10	20	16	12
10	30	25	19
10	40	32	25

The histograms summarizing the mass estimation errors, obtained from 1000 simulations in which different levels of uncertainties have been considered, are displayed in Fig. 2, while the corresponding statistics are listed in Table 3.

From the simulation results, it can be noted that, up to an uncertainty level of 40% in the SC_d, the 80% of the performed simulations show an estimation error on the fragment's mass lower than 50%. As expected, the higher the uncertainty on SC_d, the higher the error on the mass, but the number of estimations with very high errors is still limited to 20%.

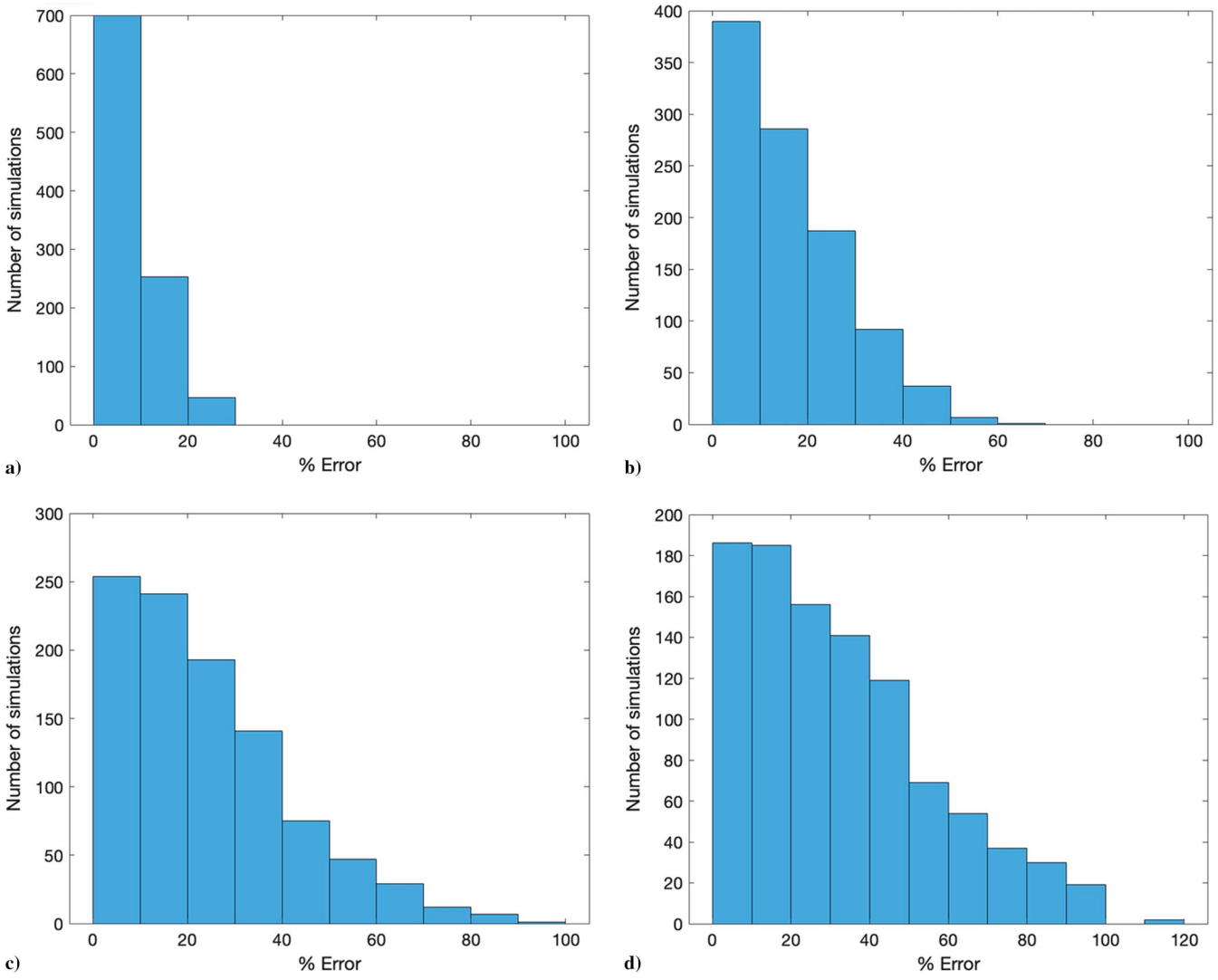

Fig. 2 Mass estimation errors for 1000 simulations in which a different standard deviation for SC_d uncertainties has been considered: a) 10%; b) 20%; c) 30%; d) 40%.

Table 4 Simulated uncertainty characteristics on aerodynamic torque, attitude, and angular velocity

Parameter	Standard deviation
Aerodynamic torque, N · m	0.001
Attitude, °	1
Angular velocity, $° \cdot s^{-1}$	0.2

Table 5 Simulation results for the moments of inertia estimation

Angular velocity uncertainty	Aerodynamic torque uncertainty	Attitude uncertainty	Mean percentage error, %
Y	N	N	5.8
N	Y	N	4.25
N	N	Y	15.5
Y	Y	Y	23.5

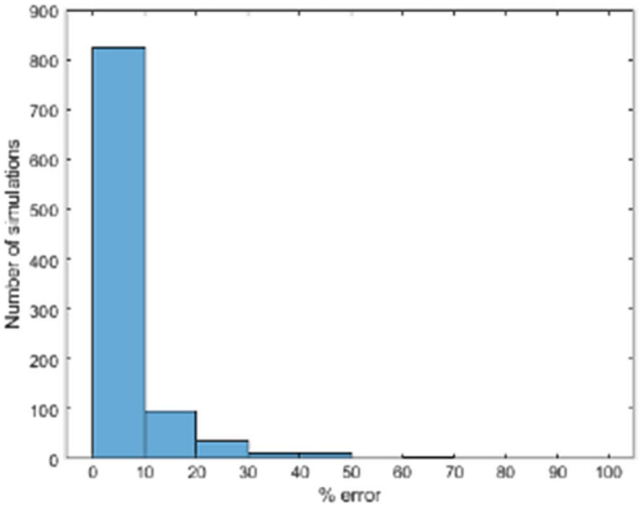

Fig. 3 Moments of inertia estimation errors for 1000 simulations in which uncertainties on the aerodynamic torque, attitude, and angular velocity are considered.

C. Moments of Inertia Estimate: Simulation Results

Regarding the inertia estimate, assuming to have more than one stereo-imaging system, the complete shape of the fragments can be reconstructed [18]. These data, along with the estimated time variation of the velocity, allow one to reconstruct the aerodynamic torque acting on the fragments. Based on this consideration, an uncertainty on the aerodynamic torque, along with uncertainties on the knowledge of both attitude and angular velocity, has been considered to quantify the performance of the proposed approach. Specifically, the standard deviations of the Gaussian white noises considered are listed in Table 4.

For each value of uncertainty, 1000 Monte Carlo simulations were performed to evaluate their effect on the moments of inertia estimate. Then, an additional 1000 simulations were performed, in which all the uncertainties were considered. The results from all simulations are listed in Table 5. Specifically, it can be noted that even when considering the combined effect of the uncertainties, a 20% accuracy can be obtained, with major contribution due to the uncertainty on the knowledge of the instantaneous attitude. Also, a histogram showing the distribution of the estimation error over the 1000 simulations is shown in Fig. 3 for the case including all the uncertainty where it can be noted that in the worst case the moments of inertia are estimated with an error of 70%.

IV. Experimental Results

To assess the performance of the proposed mass estimate approaches, experimental data were also analyzed (Fig. 4).

Specifically, the mass has been estimated with Eq. (7) and compared to the real mass for two different fragments whose trajectories were been tracked by stereovision systems.

Figures 5 and 6 depict the time variation of the estimated velocity, acceleration (computed with a first-order numerical derivative scheme), and the area projected along the x direction.

Considering a measured air density on the day of the test of 1.0128 kg/m^3 and assuming a constant drag coefficient equal to 1.2, provided by the [12], a fragment mass of 0.608 kg was estimated following the approach presented in Sec. II.A. The real mass of the fragment 0.604 kg, yielding a 0.68% estimation error.

A second test was conducted using a fragment of 0.01737 kg. Utilizing the data obtained by the stereovision system, the mass of this fragment was estimated to be 0.0172 kg, yielding a 0.88% estimation error. The time variation of velocity, acceleration, and projected area are shown in Figs. 7 and 8.

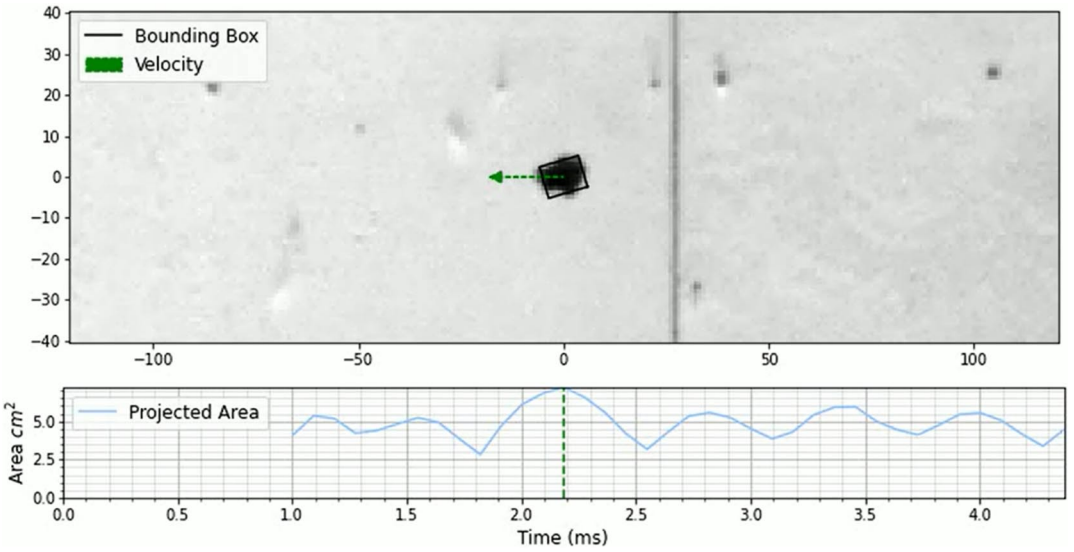

Fig. 4 Experimental data: screenshot example of a single fragment video capture, showing the assumed bounding box, estimated velocity, and projected area vs time.

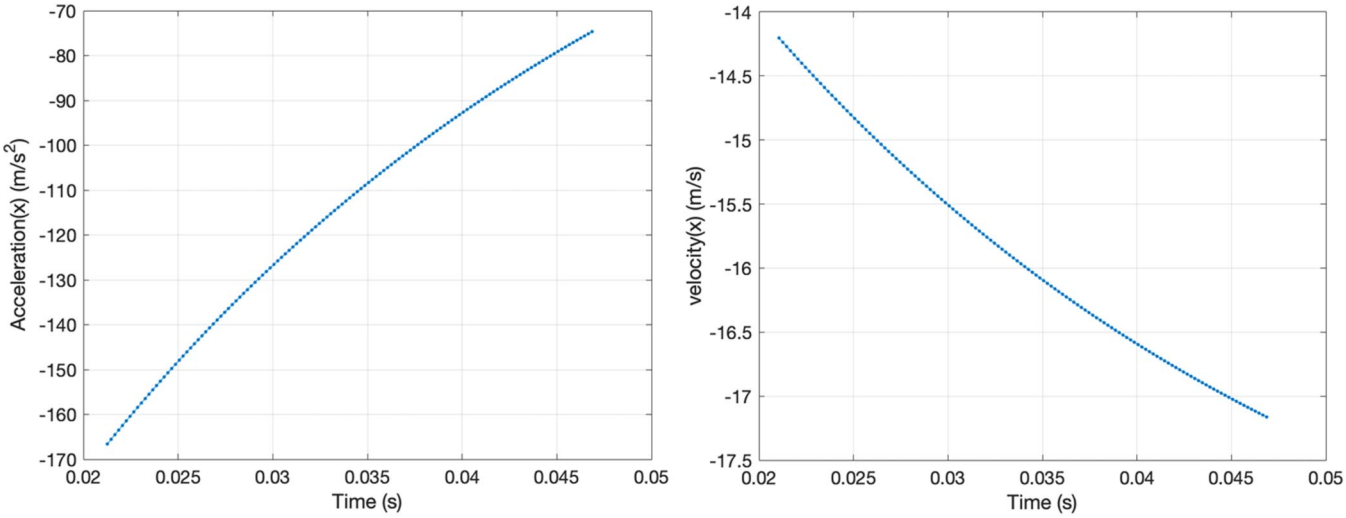

Fig. 5 Time variation of velocity (right) and acceleration (left) of the fragment along the inertia *x* axis. Test case 1.

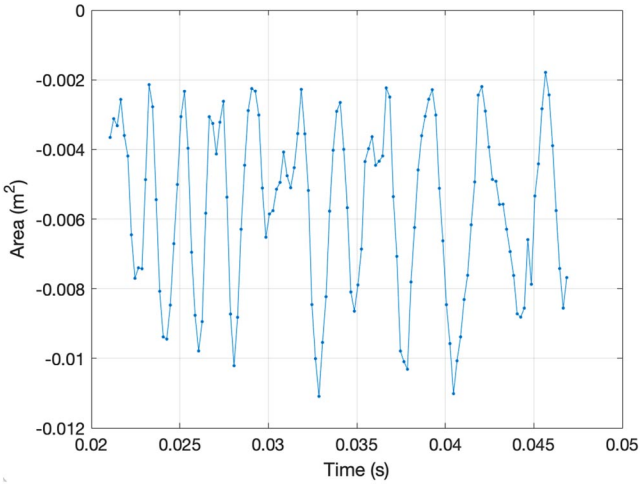

Fig. 6 Time variation of the fragment's area projected on the inertial *x* axis. Test case 1.

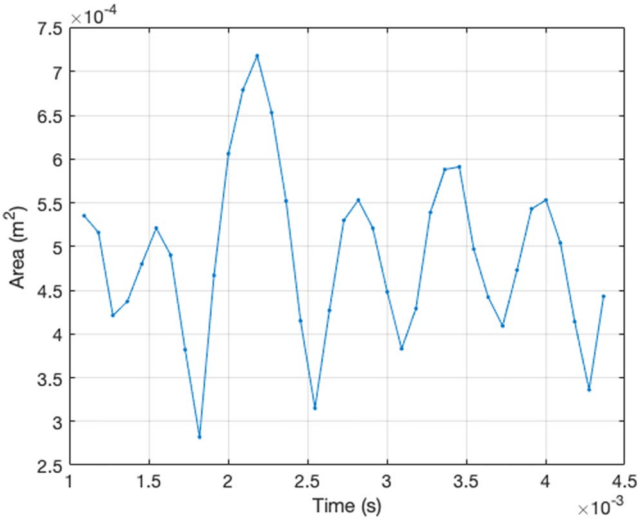

Fig. 8 Time variation of the fragment's area projected on the inertial *x* axis. Test case 2.

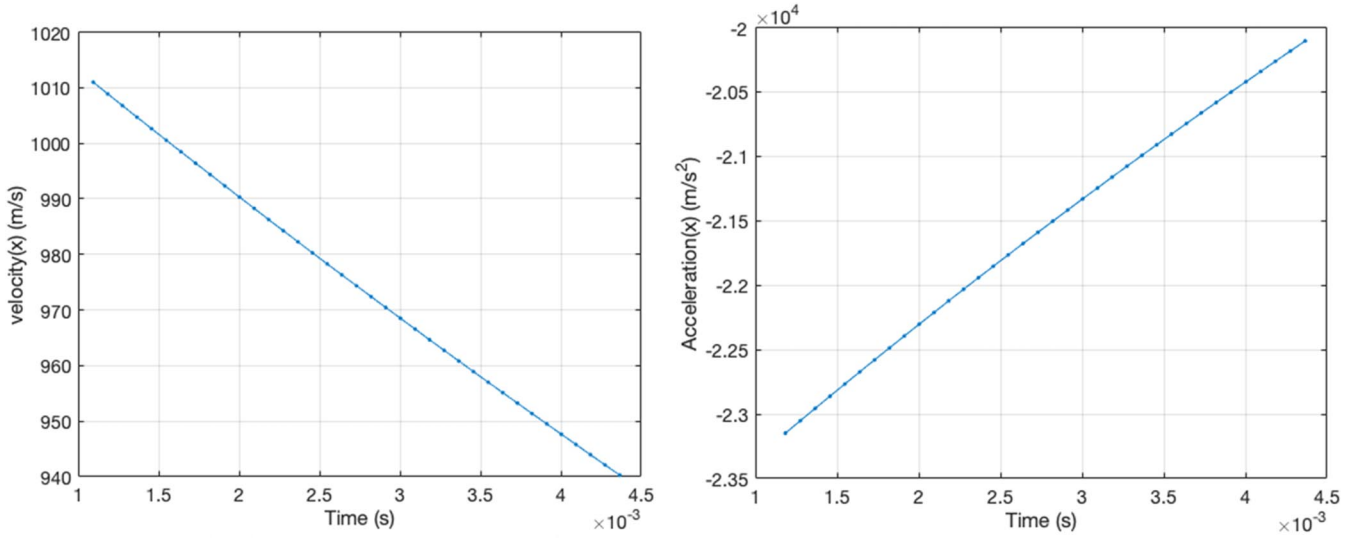

Fig. 7 Time variation of velocity (left) and acceleration (right) of the fragment along the inertia *x* axis. Test case 2.

V. Conclusions

This paper presents a strategy to estimate both mass and inertia parameters of a fragment deriving from an explosion, which can then be utilized to evaluate weapon characteristics or the impact and the danger of the fragmentation of objects (e.g., buildings, cars, bridges) due to an explosive event. In the scenarios under study, all fragments were tracked by multiple stereovision systems, capable of estimating each fragment's motion state (position, velocity, attitude, and angular velocity) and their area perpendicular to the cross-boresight direction. Using these estimates, this paper presents a strategy to estimate the mass properties, considering some simplifying assumptions. Specifically, the estimate of the mass relies on the second principle of the dynamics in which the gravity and the drag have been considered as the only external forces acting on the fragment, leading to a linear equation in which, after adopting a simplified model to determine the aerodynamic force, the only unknown parameter is the mass. However, the known parameters of the equation (i.e., velocity and cross-sectional area) are affected by uncertainties from the processing of the stereo images. Therefore, a linear system based on multiple observations has been solved to reduce the effect of the noise of the measurements on the mass estimate.

Regarding the estimation of moment of inertia matrix, an approach similar to a vision-based inertia estimation of space debris was adopted. However, in this proposed method, the fragment cannot be considered a freely tumbling rigid body since the effect of the external torque on the rotational motion cannot be neglected. In this case, the system is not homogenous, and the complete moment of inertia matrix can be determined by solving a linear system based on the expression of the angular momentum vector in the inertial frame. In the rotational motion modeling, the aerodynamic torque is the only external perturbation considered. Additionally, in this case, a linear system based on multiple observations has been built and solved with a least square approach to reduce the effect of the measurements' noise on the results.

To assess the accuracy of the presented strategies, numerical simulations were performed by representing the noise of the measurements as white Gaussian distributions to be added to the reference values. Numerical results show a maximum percent error of 20% for the inertia estimate, while for the 80% of the simulations an error lower than 50% is guaranteed on the mass estimate. Finally, some experimental data have also been exploited to assess the performance of the mass estimation procedure: in the two test cases presented, the estimation error is below 1%, proving that the uncertainties simulated for the numerical performance assessment were overconservative; i.e., the modeled uncertainties are higher than the ones observed during the experimental tests. Future work will include more accurate models allowing to reconstruct in a more accurate way the aerodynamic forces and torques experience by the fragments as well as the assessment of the performance of the inertia estimation algorithm with experimental data.

Acknowledgments

This research was made possible by 1) the Air Force Research Laboratory Summer Faculty Fellowship Program, attended by Bevilacqua in summer 2022; 2) the Air Force Office of Scientific Research, through Grant #FA9550-20-1-0200; and 3) an ERAU-Federico II collaboration.

References

[1] Mulekar, O. S., Bevilacqua, R., Jerome, E. L., and Hatch-Aguilar, T. J., "Transfer Function to Predict Warhead Fragmentation In-Flight Behavior from Static Data," *AIAA Journal*, Vol. 59, No. 11, 2021, pp. 4777–4793. https://doi.org/10.2514/1.J060226

[2] Gold, V. M., "Fragmentation Model for Large L/D (Length over Diameter) Explosive Fragmentation Warheads," *Defense Technology*, Vol. 13, No. 4, 2017, pp. 300–309. https://doi.org/10.1016/j.dt.2017.05.007

[3] Baker, W. E., Dodge, F. T., and Westine, P. S., *Joint Munitions Effectiveness Manual*, U.S. Air Force, 1969.

[4] Hay, R. F., Gibson, G. M., Lee, M. P., Padgett, M. J., and Phillips, D. B., "Four-Directional Stereo-Microscopy for 3D Particle Tracking with Real-Time Error Evaluation," *Optics Express*, Vol. 22, No. 15, 2014, Paper 18662. https://doi.org/10.1364/OE.22.018662

[5] King, S., "Camera System Captures, Analyzes Munition Detonation Data," *Air Force Material Command*, https://www.afmc.af.mil/News/Article-Display/Article/2975486/camera-system-captures-analyzes-munition-detonation-data/ [retrieved X XX XXXX].

[6] Gold, V. M., Baker, E. L., Hirlinger, J. M., and Ng, K. W., "A Method for Predicting Fragmentation Characteristics of Natural and Performed Explosive Fragmentation Munitions," Army Armament Research Development and Engineering Center, Picatinny Arsenal, NJ, Sept. 2001, ADA403989. https://doi.org/10.21236/ada403989

[7] Tipton, R. E., *The CALE User's Manual*, Version 910201, 1991.

[8] Gold, V. M., Baker, E. L., and Pincay, J. M., "Computer Simulated Fragmentation Arena Test for Assessing Lethality and Safety Separation Distances of Explosive Fragmentation Ammunitions," *Computational Ballistics III*, 2007. https://doi.org/10.2495/cbal070171

[9] Mott, N. F., "Fragmentation of Shell Cases," *Proceedings of the Royal Society of London: Series A. Mathematical and Physical Sciences*, Vol. 189, No. 1018, 1947, pp. 300–308. https://doi.org/10.1098/rspa.1947.0042

[10] Felix, D., Colwill, I., and Harris, P., "A Fast and Accurate Model for the Creation of Explosion Fragments with Improved Fragment Shape and Dimensions," *Defence Technology*, Vol. 18, No. 2, 2022, pp. 159–169. https://doi.org/10.1016/j.dt.2020.12.004

[11] Elek, P., and Jaramaz, S., "Fragment Mass Distribution of Naturally Fragmenting Warheads," *FME Transactions*, Vol. 37, No. 3, 2009, pp. 129–135.

[12] Potter, M. C., and Wiggert, D. C., *Mechanics of Fluids*, 2nd ed., Prentice-Hall, Hoboken, NJ, 1997, p. 351.

[13] Feng, Q., Zhu, Z. H., Pan, Q., and Hou, X., "Relative State and Inertia Estimation of Unknown Tumbling Spacecraft by Stereo Vision," *IEEE Access*, Vol. 6, Sept. 2018, pp. 54,126–54,138. https://doi.org/10.1109/ACCESS.2018.2872039

[14] Nocerino, A., Opromolla, R., Fasano, G., and Grassi, M., "Lidar-Based Multi-Step Approach for Relative State and Inertia Parameters Determination of an Uncooperative Target," *Acta Astronautica*, Vol. 181, April 2021, pp. 662–678. https://doi.org/10.1016/j.actaastro.2021.02.019

[15] Ge, D., Wang, D., Zou, Y., and Shi, J., "Motion and Inertial Parameter Estimation of Non-Cooperative Target on Orbit Using Stereo Vision," *Advances in Space Research*, Vol. 66, No. 6, 2020, pp. 1475–1484. https://doi.org/10.1016/j.asr.2020.05.029

[16] Wang, X., Wang, Z., and Zhang, Y., "Stereovision-Based Relative States and Inertia Parameter Estimation of Noncooperative Spacecraft," *Proceedings of the Institution of Mechanical Engineers, Part G: Journal of Aerospace Engineering*, Vol. 233, No. 7, 2018, pp. 2489–2502. https://doi.org/10.1177/0954410018782021

[17] Rawashdeh, S. A., "Attitude Analysis of Small Satellites Using Model-Based Simulation," *International Journal of Aerospace Engineering*, Vol. 2019, April 2019, pp. 1–11. https://doi.org/10.1155/2019/3020581

[18] Rawashdeh, S. A., "Attitude Analysis of Small Satellites Using Model-Based Simulation," *International Journal of Aerospace Engineering*, Vol. 2019, April 2019, Article ID 3020581.

D. Livescu
Associate Editor